Raman Linear Intensity Difference of Flow-Oriented Macromolecules: Orientation of the Indole Ring of Tryptophan-26 in Filamentous Virus *fd*

Hideo Takeuchi,*,† Motonori Matsuno,† Stacy A. Overman,‡ and George J. Thomas, Jr.*,‡

Contribution from the Pharmaceutical Institute, Tohoku University, Aobayama, Sendai 980-77, Japan, and the Division of Cell Biology and Biophysics, School of Biological Sciences, University of Missouri—Kansas City, Kansas City, Missouri 64110

Received November 22, 1995[⊗]

Abstract: A Raman linear intensity difference (RLID) method has been developed to determine orientations of chromophores in filamentous macromolecular assemblies. The method involves orientation of the filaments by hydrodynamic shear force and measurement of intensity differences between Raman spectra excited with laser polarizations parallel and perpendicular to the direction of orientation. Analysis of the RLID spectrum is simplified when the chromophore exhibits a vibrational mode for which the Raman band is enhanced by laser irradiation in resonance with a single molecular electronic transition. In the case of tryptophan, two such modes can be identified: The Raman bands corresponding to indole normal modes $\omega 2$ and $\omega 16$ gain intensity predominantly through resonance with L_a and B_b electronic transitions, respectively, when excited by laser wavelengths of 266 and 240 nm. We have oriented the filamentous bacterial virus *fd* by hydrodynamic shear force in a velocity gradient flow cell and examined the orientation of the single indole ring (tryptophan-26) in the major coat protein subunit (pVIII) of the virion. The indole ring is found to be inclined at $31 \pm 4°$ from the virion axis with its pseudo-2-fold axis at an angle of $38 \pm 6°$ to the virion axis. Using the indole ring orientation determined by the RLID method and the side chain torsion $\chi^{2,1}$ (dihedral angle Cα−Cβ−C3−C2) determined from the Raman $\omega 3$ band, the conformation of the W26 side chain in the viral coat protein has been determined. Similar analysis has been applied to the tyrosine-21 and tyrosine-24 residues of the pVIII subunit. On the basis of the present results, a molecular model is proposed for the pVIII subunit of the native *fd* assembly. The model is also consistent with data from fiber X-ray diffraction analysis and polarized Raman microspectroscopy of oriented *fd* fibers.

Introduction

Filamentous macromolecules and their assemblies can be oriented for spectroscopic analysis in a field of electric, magnetic, hydrodynamic, or mechanical force.[1−3] Among these, hydrodynamic shear force is widely used because orientation can be achieved simply by flowing a solution through a narrow gap. It is particularly advantageous for structural studies of biological macromolecules in an aqueous environment. Optical properties of oriented aqueous biomolecules have been examined by ultraviolet (UV) and visible absorption spectroscopy employing linearly polarized light. The measured difference in absorption intensity for two orthogonal polarizations, which is termed the linear dichroism (LD), can be exploited to determine the direction of a chromophore transition dipole moment with respect to the axis of flow orientation. For example, the angles of inclination of purine and pyrimidine base planes in double helical DNA and the orientations of drug or protein chromophores which bind specifically to DNA have been extensively studied by the flow LD method in combination with UV and visible absorption spectroscopy.[2]

Flow LD spectroscopy is particularly advantageous when the absorption band of interest is well resolved from interfering absorption of other chromophores. However, if extensive spectral overlap occurs, such as between absorption bands of different aromatic side chains in a protein, separation of the overlapping bands may not be straightforward and determination of chromophore orientation geometry may not be possible. Although site-directed mutagenesis, in which a potentially interfering aromatic protein side chain (absorbing chromophore) is replaced by a nonabsorbing aliphatic side chain, can sometimes circumvent the problem of band overlap,[4] this strategy is not always applicable. Even when site-directed mutagenesis is feasible, it is still possible that side chain substitution can alter the native structure of the protein molecule and complicate the structural interpretation. An alternative approach is to combine flow LD with a spectroscopic probe of greater selectivity than is obtainable by electronic absorption spectroscopy. One such probe is vibrational spectroscopy.

In the case of vibrational spectroscopy (Raman scattering or infrared absorption), the spectral bands are less subject to extensive overlap owing to their much narrower band widths ($\sim$10 cm^{-1}) in comparison to those of electronic absorption spectroscopy ($\sim 10^2-10^3$ cm^{-1}). In the particular case of resonance Raman spectroscopy, the likelihood of band overlap is further reduced because Raman scattering is limited strictly to vibrational modes of the chromophore for which the excited state is in resonance with the laser excitation wavelength.

* Authors to whom correspondence may be addressed.
† Tohoku University.
‡ University of Missouri-Kansas City.
⊗ Abstract published in *Advance ACS Abstracts,* April 1, 1996.
(1) Wada, A. *Appl. Spectrosc. Rev.* **1972**, *6*, 1−30.
(2) (a) Nordén, B. *Appl. Spectrosc. Rev.* **1978**, *14*, 157−248. (b) Nordén, B.; Kubista, M.; Kurucsev, T. *Q. Rev. Biophys.* **1992**, 51−170.
(3) Schellman, J.; Jensen, H. P. *Chem. Rev.* **1987**, 1359−1399.
(4) Hagmar, P.; Nordén, B.; Baty, D.; Chartier, M.; Takahashi, M. *J. Mol. Biol.* **1992**, 1193−1205.
(5) Carey, P. R. *Biochemical Applications of Raman and Resonance Raman Spectroscopies*; Academic Press: London, 1982; p 262.

0002-7863/96/1518-3498$12.00/0

(Further background is given by Carey.[5]) Thus, resonance Raman spectroscopy is especially well suited to structural analysis of flow-oriented macromolecules and their assemblies.

The first application of flow orientation in Raman spectroscopy was described by Tsuboi *et al.*,[6] who analyzed the binding mode of the antitumor drug aclacinomycin A to double helical DNA. These authors employed visible (488 nm) laser excitation of the Raman spectrum, close to resonance with absorption of the aclacinomycin chromophore (437 nm), and compared Raman intensities of in-plane vibrations of the chromophore for polarizations parallel and perpendicular to the direction of DNA orientation. The stronger Raman intensities observed in the spectrum excited with perpendicular polarization led to the proposal of an intercalation model for the drug−DNA complex.[6] Although qualitative, the results established the feasibility of the method and demonstrated the potential of resonance Raman spectroscopy in combination with flow orientation as an effective structural probe of biological macromolecular complexes.

In the present work we describe a novel velocity gradient flow cell which can be exploited for structural study of biological assemblies by ultraviolet resonance Raman (UVRR) spectroscopy using the 180° back-scattering geometry. The experimental design incorporates switching of UV laser polarizations, enabling the rapid tandem collection of Raman spectra with excitations alternately parallel and perpendicular to the direction of flow orientation. The Raman intensity difference measured between the two polarizations may be termed the Raman linear intensity difference (RLID). We derive an equation which relates the RLID to the orientation of the UVRR chromophore. We also describe a procedure for compensating the experimentally measured RLID for rotational diffusion which may cause imperfect alignment of the chromophores. The RLID-UVRR technology and its application to a biological macromolecular assembly oriented by hydrodynamic shear force is illustrated for the filamentous bacterial virus *fd* in dilute aqueous solution.

The virus *fd* is a member of the *Ff* class of bacteriophages (inovirus), which includes the phages *f1* and *M13*. The virion is a long (≈880 nm) and thin (≈6-nm diameter) particle, in which a single-stranded DNA (ssDNA) loop of 6410 nucleotides is sheathed by 2700 copies of a 50 residue subunit (major coat protein, pVIII). Previous structural studies (Marvin *et al.*[7] and references therein) have shown that the pVIII subunit is uniformly α-helical and layered along the filament axis with 5-fold rotational symmetry and an approximate 2-fold screw axis. Polarized Raman microspectroscopy of *fd* fibers has also revealed that, on average, the axis of the pVIII α-helix is aligned close to parallel to the filament axis.[8] Although a high-resolution structure is not available, interactions and environments of the unique tryptophan (W26)[9] and two tyrosines (Y21, Y24)[10,11] of pVIII have been investigated using Raman spectroscopy in combination with residue-specific isotope labeling and site-directed mutagenesis. More detailed knowledge of pVIII side chain conformations and environments should enable more accurate modeling of protein−protein and protein−DNA interfaces within the virion. This information is essential to understanding filamentous virus assembly and disassembly mechanisms.

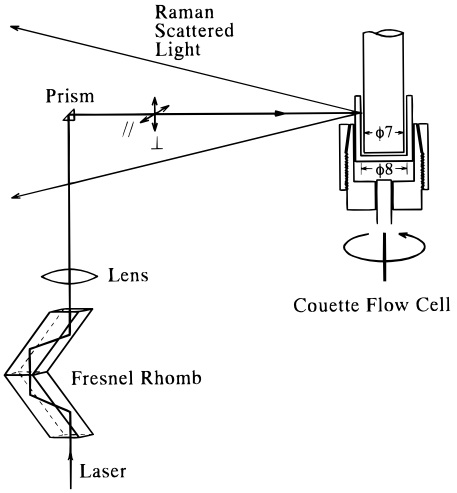

Figure 1. Schematic representation of the apparatus for measurement of Raman linear intensity difference. The Couette flow cell consists of a spinning outer quartz cylinder (8.0 mm i.d.) and a stationary inner quartz rod (7.0 mm o.d.). The Fresnel rhomb rotates the polarization of the incident laser light. The Raman scattering from oriented molecules in the Couette flow cell is collected with Cassegrain mirror optics (not shown).

Here we report the first UVRR spectra of flow-oriented *fd* and interpret the RLID measurements to reveal the orientation of the indole ring of residue W26 in the native aqueous virion. The results are compared with and discussed in relation to a similar determination on *fd* fibers by Raman microspectroscopy.[12]

Experimental Methods

A diagram of the Couette-type flow cell used in this study is shown in Figure 1. The basic principle of operation is the establishment of a velocity gradient in a thin annular layer (0.5 mm) of a solution of filamentous particles contained between a rotating outer cylinder (8.0 mm inner diameter) and a stationary inner rod (7.0 mm outer diameter). Both the cylinder and rod are fabricated from synthetic quartz to achieve optical transparency to a low-wavelength limit of 180 nm. When the number of revolutions per minute (rpm) of the outer cylinder is N (or $N/60$ revolutions per second), the liquid flow velocity is $2\pi N/15$ mm s^{-1} on the outer surface of the annular ring and zero at the inner surface, thus establishing the velocity gradient $G = 4\pi N/15$ s^{-1} within the annular ring. The velocity gradient generates a shear force which aligns the long axis of the filamentous particles along the direction of flow. Advantages of this Couette arrangement over the alternative Wada−Kozawa design,[13] which consists of inner rotating and outer stationary cylinders, are the uniformity of its velocity gradient throughout the liquid and its capacity to achieve higher velocity gradients with simple laminar flow.[14] An additional feature of the Couette cell, which is of particular importance to resonance Raman spectroscopy, is that the more slowly moving particles near the inner stationary wall are less intensely irradiated than the more rapidly moving particles near the rotating outer cylinder. Thus, the undesirable local heating of the sample from laser irradiation is more easily controlled.

The UV laser and UV Raman spectrometer used in this study have been described in detail.[15] Briefly, radiation at 266 nm is generated

(6) (a) Tsuboi, M.; Ikeda, T.; Shindo, H. *Chem. Pharm. Bull.* **1987**, *35*, 4405−4409. (b) Tsuboi, M. In *Spectroscopy of Biological Molecules−New Advances*; Schmid, E. D., Schneider, F. W., Siebert, F., Eds.; Wiley: New York, 1987; pp 367−372.

(7) (a) Marvin, D. A.; Hale, R. D.; Nave, C.; Helmer-Citterich, M. *J. Mol. Biol.* **1994**, *235*, 260−286. (b) Marvin, D. A. *Int. J. Biol. Macromol.* **1990**, *12*, 125−138.

(8) Overman, S. A.; Tsuboi, M.; Thomas, G. J., Jr. *J. Mol. Biol.* Submitted for publication.

(9) Aubrey, K. L.; Thomas, G. J., Jr. *Biophys. J.* **1991**, *60*, 1337−1349.

(10) Overman, S. A.; Aubrey, K. L.; Vispo, N. S.; Cesareni, G.; Thomas, G. J., Jr. *Biochemistry* **1994**, *33*, 1037−1042.

(11) Overman, S. A.; Thomas, G. J., Jr. *Biochemistry* **1995**, *34*, 5440−5451.

(12) Tsuboi, M.; Overman, S. A.; Thomas, G. J., Jr. *Biochemistry*. Submitted for publication.

(13) Wada, A.; Kozawa, S. *J. Polym. Sci. Part A* **1964**, *2*, 853−864.

(14) (a) Taylor, G. I. *Proc. R. Soc. London A* **1936**, *157*, 546−564. (b) Taylor, G. I. *Proc. R. Soc. London A* **1936**, *157*, 565−578.

(15) Takeuchi, H.; Harada, I. *J. Raman Spectrosc.* **1990**, *21*, 509−515.

by frequency quadrupling the 1064-nm pulses from a Nd:YAG laser (Quanta Ray DCR-3G) operating at a 30 Hz repetition rate. A hydrogen gas Raman shifter (Quanta Ray RS-1) generates 240-nm radiation from the 266-nm pulses. The laser beam (*ca.* 1 mW) is focused onto the sample solution in the flow cell annulus at a right angle to the cylinder cell wall and the Raman photons are collected in the back-scattering geometry (180°) with custom designed Cassegrain optics. The Raman photons are dispersed by a double monochromator equipped with a quartz polarization scrambler (Jasco CT-80D) and detected by an intensified diode array (Princeton Instruments D/SIDA-700IG). The plane of polarization of the incident laser beam is directed by a Fresnel rhomb half-wave prism (Sigma Optical Co.) either parallel or perpendicular to the direction of sample flow.

The quality of laser polarization and the performance of polarization devices was checked by measuring depolarization ratios (ρ) of CCl_4 Raman bands with a Polacoat analyzer. Measured ρ values for the Raman bands of CCl_4 at 459 and 790/762 cm^{-1} (doublet) were respectively 0.05 ± 0.02 and 0.76 ± 0.03, essentially identical to the expected values (0 and 0.75, respectively) for a tetrahedral molecule. Raman ρ values for the amino acid tryptophan and tyrosine were recorded in the same manner.

The bacteriophage *fd* was grown on *Escherichia coli* strain Hfr3300 and purified as described.[9] Deuterated tryptophan (L-tryptophan-*2,4,5,6,7-d*$_5$, hereafter abbreviated dW) was incorporated into pVIII by use of M9 minimal medium in which L-tryptophan was replaced by dW.[10] Purified pellets of normal *fd* and its deuterated counterpart [*fd*(dW)] were suspended in 10 mM Tris (pH 7.8) at a concentration of 1 mg/mL. Approximately 120 μL of the virus solution was placed in the flow cell and the outer cylinder was rotated (G, s^{-1}) at 800 (670), 1200 (1005), 1600 (1340), 2500 (2094), or 3600 rpm (3016). The laser polarization was switched from parallel to perpendicular, or *vice versa*, every 1 min and the Raman signals with specific laser polarizations ($I_{\parallel}$ and $I_{\perp}$, respectively) were accumulated in separate memories of a personal computer. (Frequent polarization switching minimizes the influence of laser power fluctuations.) The $I_{\parallel}$ and $I_{\perp}$ Raman spectra of virus solutions in the region 1750−950 cm^{-1} were each accumulated for 12 min, and remained unchanged over this time interval. The spectrometer was then advanced to the O−H stretching region (3800−3000 cm^{-1}) and the $I_{\parallel}$ and $I_{\perp}$ spectra were again recorded in a similar manner. The Raman band of H_2O near 3400 cm^{-1} in each spectrum was used as an internal intensity standard to correct for any small instrumental bias in intensity measurements. Because the solvent molecules are not oriented by shear force, they are expected to give identical Raman intensities near 3400 cm^{-1} with the two polarizations. Following the measurements described above, each sample was replaced by a fresh one. The spectra reported here are the averages of those recorded on 8−12 identical samples.

Theoretical Treatment

Generally, the Raman scattering tensor $\alpha_{LL'}$ (L, $L' = X, Y, Z$) expressed in the laboratory coordinate system is related to the Raman tensor $\alpha_{mm'}$ (m, $m' = x, y, z$) in the molecular coordinate system as follows:[16]

$$\alpha_{LL'} = \sum_{LL'} \Phi_{Lm}\Phi_{L'm'}\alpha_{mm'} \qquad (1)$$

where Φ_{Lm} ($\Phi_{L'm'}$) is the direction cosine between the L (L') and m (m') axes. When the molecule is excited with light polarized along L', the intensity of Raman scattering with polarization along L is proportional to $|\alpha_{LL'}|^2$. The direction cosine Φ_{Lm} can be determined from the observed Raman intensity if $\alpha_{mm'}$ has a simple form.[17] This is the case in resonance Raman scattering because most elements of the $\alpha_{mm'}$ tensor vanish. In particular, when the Raman intensity arises from resonance with an allowed electronic transition (Albrecht **A**-term resonance)[18] and both the ground and excited electronic states are nondegenerate, only one diagonal element of the Raman tensor is nonzero.[19] In such a case, eq 1 is greatly simplified and Φ_{Lm} may be determined from the observed Raman intensity.

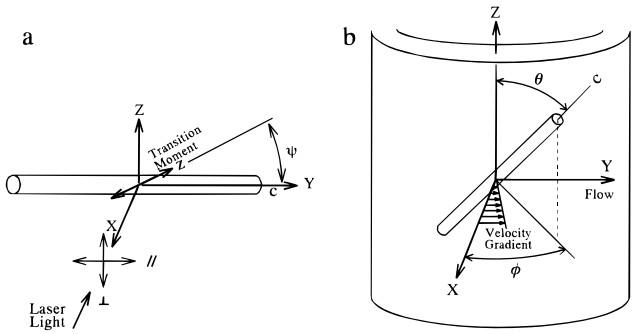

Figure 2. (a) Arrangement for measurement of the Raman linear intensity difference. The cylinder represents a filamentous particle oriented with its axis (c) along the direction of flow (Y). The incident laser light with polarization parallel (||) or perpendicular (⊥) to Y is impingent from the X direction and Raman photons are collected in the back-scattering (180°) geometry. ψ is the angle between the chromophore transition moment (z) and Y. (b) Coordinate system for analysis of orientation of filamentous particles in a Couette flow cell.

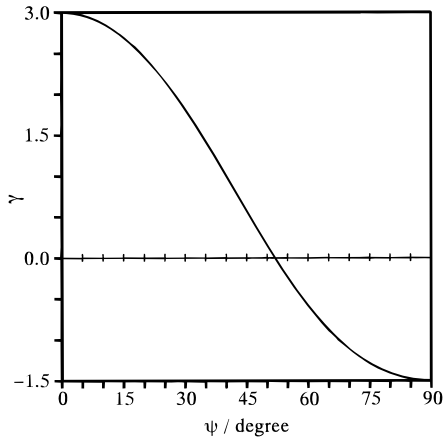

Figure 3. Graphical relationship between the reduced Raman linear intensity difference (γ) and the angle of inclination (ψ) of the transition moment with respect to the flow direction. Derived from eq 4.

Here we assume that the macromolecular assembly (*fd* filament) flows in the field of the velocity gradient and the transition moment responsible for the resonance Raman intensity of a molecular vibration forms an angle ψ with respect to the filament axis. If the molecule-fixed z axis is selected as the direction of the transition moment, only the α_{zz} component of the Raman tensor is nonzero for the case of nondegenerate **A**-term resonance. When filament alignment is along the direction of flow (Y), the experimental arrangement (Figure 1) leads to the molecular orientation shown in Figure 2a, where X is the axis along which both the incident and Raman scattered light are propagated. After cylindrical averaging (uniaxial orientation), the experimental Raman intensities, $I_{\parallel}$ and $I_{\perp}$, which correspond respectively to incident laser polarizations parallel (along Y) and perpendicular (along Z) to the flow direction, are given by:

$$I_{\parallel} = C\langle\alpha_{YY}^2 + \alpha_{ZY}^2\rangle = C(\cos^4\psi + \cos^2\psi)\,\alpha_{zz}^2/2 \qquad (2)$$

$$I_{\perp} = C\langle\alpha_{YZ}^2 + \alpha_{ZZ}^2\rangle = C\,(-\cos^4\psi - 2\cos^2\psi + 3)\alpha_{zz}^2/8 \qquad (3)$$

where C is a constant independent of the laser polarization and the angle brackets denote averaging over all rotations around the filament axis. Comparison of these equations shows that $I_{\parallel} = I_{\perp}$ at the "magic" angle of $\psi = 52°$. For $\psi < 52°$, $I_{\parallel} > I_{\perp}$; otherwise $I_{\parallel} < I_{\perp}$. The reduced RLID, γ, may be defined as:

(16) Wilson, E. B., Jr.; Decius, J. C.; Cross, P. C. *Molecular Vibrations*; McGraw-Hill: New York, 1955; pp 34−53.

(17) Higgs, P. W. *Proc. R. Soc. London A* **1953**, *220*, 472−485.

(18) (a) Albrecht, A. C. *J. Chem. Phys.* **1961**, *34*, 1476−1484. (b) Tang, J.; Albrecht, A. C. In *Raman Spectroscopy, Theory and Practice*; Szymansky, H. A., Ed.; Plenum: New York, 1970; Vol. 2, pp 33−68.

(19) Behringer, J. In *Raman Spectroscopy, Theory and Practice*; Szymansky, H. A., Ed.; Plenum: New York, 1967; Vol. 1, pp 168−223.

$$\gamma = \frac{3(I_{\parallel} - I_{\perp})}{I_{\parallel} + 2I_{\perp}} = \frac{3(5\cos^4\psi + 6\cos^2\psi - 3)}{2(\cos^4\psi + 3)} \quad (4)$$

The relationship between γ and ψ is plotted in Figure 3.

Because perfect uniaxial alignment of molecules or their assemblies cannot usually be achieved by the flow orientation method, the sample inevitably contains unaligned particles. We define f as the fraction of perfectly aligned particles and $1 - f$ as the fraction of randomly oriented particles. The Raman intensity of the ensemble may be expressed as a sum of both fractions. Since the Raman intensity from the randomly oriented fraction is independent of the polarization of incident light (in the 180° back-scattering geometry), eq 5 gives the polarized Raman intensities for this fraction.[16]

$$I_{\parallel} = I_{\perp} = 4\alpha_{zz}^2/15 \quad (5)$$

Combining eqs 4 and 5, we obtain the following general expression for γ of an ensemble of partially aligned particles.

$$\gamma = \frac{15f(5\cos^4\psi + 6\cos^2\psi - 3)}{10f(\cos^4\psi + 3) + 32(1 - f)} \quad (6)$$

Equation 6 reduces to eq 4 when $f = 1$. Since two unknown parameters, ψ and f, are contained in eq 6, a single measurement of γ is not sufficient to determine ψ. However, if the value of γ can be estimated for the limiting case of perfect alignment ($f = 1$) through multiple measurements at different velocity gradients, the angle ψ can be determined from eq 4 or Figure 3.

Peterlin and Stuart[20] formulated an orientation distribution function $F(\theta,\phi)$ for ellipsoids in a Couette flow cell, where θ and ϕ are angles representing the orientation of the major axis (c) of the ellipsoid (Figure 2b). The distribution function is expressed (eq 7) as a power series in the shape parameter $r = (p^2 - 1)/(p^2 + 1)$, where p is the axial ratio between the long and short axes of the ellipsoid. For a thin filament, $p \gg 1$ and $r \approx 1$.

$$F(\theta,\phi) = \sum_{i=0}^{\infty} r^i \left[(1/2)\sum_{n=0}^{\infty} a_{n0,i}P_{2n}(\cos\theta) + \sum_{n=1}^{\infty}\sum_{m=1}^{n}(a_{nm,i}\cos 2m\phi + b_{nm,i}\sin 2m\phi)P_{2n}^{2m}(\cos\theta)\right] \quad (7)$$

In eq 7, P_{2n} and P_{2n}^{2m} are respectively the Legendre polynomial and associated Legendre polynomial, and the coefficients $a_{nm,i}$ and $b_{nm,i}$ are functions of the reduced velocity gradient G/D_r, where D_r is the rotational diffusion constant. If we assume this distribution function, the mean square direction cosines ($\langle\Phi_{Lc}^2\rangle$, $L = X, Y, Z$) of the ellipsoid major axis, c, with respect to the laboratory axes are related to the coefficients of eq 7 as follows:

$$\langle\Phi_{Xc}^2\rangle = \langle\sin^2\theta\cos^2\phi\rangle = 1/3 - (2\pi/15)\sum_{i=0}^{\infty} a_{10,i}r^i + (8\pi/5)\sum_{i=0}^{\infty} a_{11,i}r^i$$

$$\langle\Phi_{Yc}^2\rangle = \langle\sin^2\theta\sin^2\phi\rangle = 1/3 - (2\pi/15)\sum_{i=0}^{\infty} a_{10,i}r^i - (8\pi/5)\sum_{i=0}^{\infty} a_{11,i}r^i$$

$$\langle\Phi_{Zc}^2\rangle = \langle\cos^2\theta\rangle = 1/3 + (4\pi/15)\sum_{i=0}^{\infty} a_{10,i}r^i \quad (8)$$

Recurrence formulas to evaluate $a_{nm,i}$ and $b_{nm,i}$ in eq 7 have been given by Peterlin[20] and numerical calculations of these coefficients have been made for particular values of nm,i and G/D_r.[21] Here, we have computed $\langle\Phi_{Lc}^2\rangle$ values for an infinitesimally thin cylinder ($r = 1$) with G/D_r in the range 1−2000, in order to find the asymptotic behavior of the orientation distribution at very high G/D_r when the filament is expected to be aligned along the flow direction. Numerical calculations of $a_{10,i}$ and $a_{11,i}$ were performed on an NEC personal computer using a program coded in QuickBASIC 4.5 (Microsoft Inc.) and the summation over i was truncated when the error was estimated to be less than 0.1%. The computation converged rapidly for small G/D_r but took weeks for very large G/D_r.

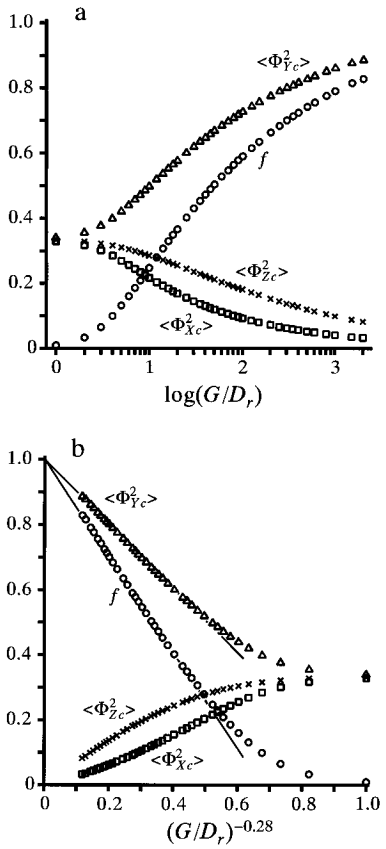

Figure 4. Dependence of the degree of uniaxial alignment (f, as defined by eq 9) on the reduced velocity gradient G/D_r: (a) semilogarithmic plot; (b) plot against $(G/D_r)^{-0.28}$. Here, $\langle\Phi_{Lc}^2\rangle$ ($L = X, Y, Z$) represents the mean square direction cosine of the filament axis (c) with respect to the laboratory fixed axis. The plotted quantities are dimensionless. The straight lines in (b) show least-squares fits to the data.

Results

1. Thin Filament Orientation in a Couette Flow Cell. Figure 4a shows a semilogarithmic plot of the mean square direction cosines, $\langle\Phi_{Lc}^2\rangle$ ($L = X, Y, Z$), calculated for 39 values of G/D_r in the 1−2000 region by use of eqs 7 and 8. At very low G/D_r, the $\langle\Phi_{Lc}^2\rangle$ values are all close to $^1/_3$, corresponding to completely unaligned states. As G/D_r increases, $\langle\Phi_{Yc}^2\rangle$ approaches 1, while both $\langle\Phi_{Xc}^2\rangle$ and $\langle\Phi_{Zc}^2\rangle$ approach 0. Extrapolation to infinite G/D_r corresponds to perfect alignment of the filaments. The degree of alignment (f) at any arbitrary value of G/D_r may be related to $\langle\Phi_{Lc}^2\rangle$ by eq 9.

$$f = \langle\Phi_{Yc}^2\rangle - (1/2)(\langle\Phi_{Xc}^2\rangle + \langle\Phi_{Zc}^2\rangle) \quad (9)$$

The f values calculated with eq 9 are also plotted in Figure 4a. Analysis of the relationship between f and G/D_r shows that f can be approximated as a linear function of $(G/D_r)^{-0.28}$ for

(20) (a) Peterlin, A. *Z. Phys.* **1938**, *111*, 232−236. (b) Peterlin, A.; Stuart, H. A. *Z. Phys.* **1939**, *112*, 1−19.

(21) (a) Wada, A. *Biopolymers* **1964**, *2*, 361−380. (b) Scheraga, H. A.; Edsall, J. T.; Gadd, J. O., Jr. *J. Chem. Phys.* **1951**, *19*, 1101−1108. (c) Nakagaki, M.; Heller, W. *J. Chem. Phys.* **1975**, *62*, 333−340.

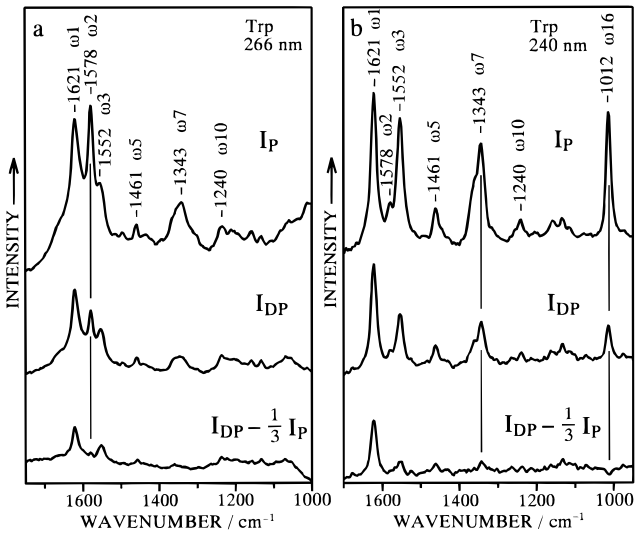

Figure 5. Polarized (I_p) and depolarized (I_{dp}) Raman spectra and their computed differences [$I_{dp} - (1/3)I_p$] for the amino acid L-tryptophan (1 mM in H_2O) excited at (a) 266 and (b) 240 nm.

G/D_r values above 10 [i.e., $(G/D_r)^{-0.28} < 0.5$], as shown in Figure 4b. $\langle \Phi_{Yc}^2 \rangle$ also exhibits linear dependence on $(G/D_r)^{-0.28}$. The reduced RLID, γ, is related to f by eq 6. While the denominator of eq 6 is not sensitive to f, the numerator is directly proportional to f. Thus, the γ value is also expected to be a linear function of $(G/D_r)^{-0.28}$, and we can estimate γ in the case of perfect alignment by plotting the experimental γ values against $(G/D_r)^{-0.28}$, or simply against $G^{-0.28}$ because the rotational diffusion constant D_r is independent of the velocity gradient.

The orientation angle ψ of the chromophore transition moment can be obtained from the γ value at infinite G by use of eq 4. For the case of pump-driven flow through a thin rectangular cell, LD in UV absorption is found to be proportional to $\bar{G}^{-1/3}$ or $\bar{G}^{-1/2}$, where $\bar{G}$ denotes the velocity gradient averaged over the cross section of the cell.[22,23] Interestingly, despite differences in the methods of flow orientation and spectroscopic detection, the empirically observed dependence on G is analogous to the theoretical dependence proposed here.

2. Raman Bands of Tryptophan Enhanced by A-Term Resonance. In order to obtain the orientation angle ψ from the measured γ values by the method described above, the Raman band to be used for the analysis must fulfill the requirement that the band is resonance enhanced by a nondegenerate **A**-term mechanism so that the Raman tensor consists of a single nonzero diagonal element. In such a case, the measured depolarization ratio ρ should be 1/3 for a sample consisting of randomly oriented molecules.[19] On the other hand, if the tensor has an additional diagonal element which is up to 10% of the magnitude of the primary diagonal element, then $0.28 < \rho < 0.39$. Accordingly, if a resonance enhanced Raman band exhibits ρ in this range, it may be concluded, to a good approximation, that the Raman band gains intensity predominantly (i.e., at least 90%) via the **A**-term mechanism. We have examined the ρ values of Raman bands of L-tryptophan for possible use in RLID studies.

In Figure 5a we show the polarized (I_p, top trace) and depolarized (I_{dp}, middle trace) Raman spectra of aqueous L-tryptophan excited at 266 nm and their corresponding difference spectrum ($I_{dp} - I_p/3$, bottom trace). The intense I_p band

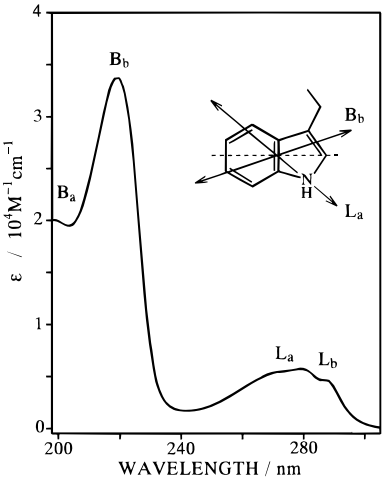

Figure 6. UV absorption spectrum of L-tryptophan (1 mM in H_2O) in the wavelength interval 200−300 nm.

at 1578 cm^{-1}, denoted $\omega 2$,[24] exhibits $\rho = 0.36 \pm 0.03$, indicating that one diagonal element of the Raman tensor is the predominant contributor. The indole ring of tryptophan shows a broad absorption band in the region 260−290 nm (Figure 6), which is ascribed to overlap of the stronger L_a (≈275 nm) and weaker L_b (≈290 nm) transitions.[25] Excitation profiles show that the $\omega 2$ Raman band is enhanced in resonance with the L_a and L_b transitions, but not with the very strong B_b transition located at much shorter wavelength (218 nm).[26,27] Thus, the contribution of the B_b transition to the 266-nm-excited Raman band of $\omega 2$ is negligible. Because the L_a absorption band has a greater sensitivity to solvent perturbation than the L_b absorption band,[25a] we examined the effect of solvent upon the $\omega 2$ excitation profile in the region 240−270 nm using an excimer dye laser and found that the $\omega 2$ Raman intensity follows closely the solvent-induced change of L_a absorption intensity (data not shown). This observation gives support to the conclusions that the $\omega 2$ Raman intensity arises from resonance with the L_a transition when excited at 266 nm, and that the $\omega 2$ Raman tensor has only one diagonal element associated with the L_a transition.

Polarized (I_p) and depolarized (I_{dp}) Raman spectra of L-tryptophan excited at 240 nm are shown in Figure 5b together with their difference spectrum ($I_{dp} - I_p/3$). Of the several bands enhanced at this excitation wavelength, the sharp band at 1012 cm^{-1} ($\omega 16$) exhibits $\rho \approx 1/3$ (=0.28 ± 0.02). Asher *et al.*[26] reported $\rho = 0.30$ for $\omega 16$ excited at 235 nm and concluded that the $\omega 16$ mode gains intensity through resonance with the B_b transition by a non-degenerate **A**-term mechanism. This appears to be the case also with 240-nm excitation. Accordingly, the $\omega 16$ band can serve as a probe of the B_b transition in UVRR-RLID using 240-nm excitation. The broad band at 1343 cm^{-1} ($\omega 7$) exhibits $\rho = 0.41 \pm 0.04$, which is close to $^1/_3$, suggesting a dominant contribution of the B_b transition to the $\omega 7$ intensity. However, the $\omega 7$ band is also enhanced in resonance with the L_a and L_b transitions.[26] (See Figure 5a, for example.) The $\omega 7$ intensity in the spectrum excited at 240 nm

(22) Cavalieri, L. F.; Rosenberg, B. H.; Rosoff, M. *J. Am. Chem. Soc.* **1956**, *78*, 5235−5238.
(23) Clack, B. A.; Gray, D. M. *Biopolymers* **1992**, *32*, 795−810.
(24) (a) Harada, I.; Takeuchi, H. In *Spectroscopy of Biological Systems*; Clark, R. J. H., Hester, R. E., Eds.; John Wiley and Sons, New York, 1986; pp 113−175. (b) Takeuchi, H.; Harada, I. *Spectrochim. Acta Part A* **1986**, *42*, 1069−1078.
(25) (a) Weber, G. *Biochem. J.* **1960**, *75*, 335−345. (b) Strickland, E. H.; Horwitz, J.; Billups, C. *Biochemistry* **1970**, *9*, 4914−4921.
(26) (a) Asher, S. A.; Ludwig, M.; Johnson, C. R. *J. Am. Chem. Soc.* **1986**, *108*, 3186−3197. (b) Sweeney, J. A.; Asher, S. A. *J. Phys. Chem.* **1990**, *94*, 4784−4791.
(27) (a) Fodor, S. P. A.; Copeland, R. A.; Grygon, C. A.; Spiro, T. G. *J. Am. Chem. Soc.* **1989**, *111*, 5509−5517. (b) Su, C.; Wang, Y.; Spiro, T. G. *J. Raman Spectrosc.* **1990**, *21*, 435−440.

may contain additional contributions from the L_a and L_b transitions and may not be a very appropriate probe of the B_b transition. The 1621- (ω1) and 1552-cm^{-1} (ω3) bands are also enhanced in resonance with the B_b transition, although the B_a transition at 195 nm also contributes to their intensities.[27] Evidently, more than one Raman tensor element may be responsible for the ω1 and ω3 bands excited at 240 nm because the ρ values deviate significantly from 1/3. Thus, although the ω1 and ω3 bands are intense with 240-nm excitation, they cannot be used effectively as probes of the B_b transition. In summary, the resonance Raman intensities of ω2 (266 nm) and ω16 (240 nm) are useful for examining by RLID orientation angles of the L_a and B_b transition moments, respectively.

3. Raman Linear Intensity Difference of the *fd* Virus. The *fd* virion can be approximated as a semirigid thin rod with axial ratio $p \approx 100$ and shape parameter $r \approx 1$.[28] The 2700 copies of major coat protein (pVIII) and the encapsulated ssDNA genome represent about 88% and 12%, respectively, of the virion mass. The pVIII subunit is modeled as a continuous α-helix, oriented roughly parallel to the virion axis.[7,8,28,29] The single tryptophan (W26) is located within a hydrophobic box at the middle of the 50-residue sequence. There is considerable interest as to the side chain conformation and interactions of W26 in the native virus assembly.[7,8,30] Here, we apply the newly developed RLID method to *fd* in dilute aqueous solution to ascertain the orientation of the W26 side chain.

Figure 7 shows Raman spectra excited at 266 nm on flow-oriented *fd* at $G = 3016$ s^{-1}. The upper two traces, a and b, were obtained respectively with laser polarizations parallel ($I_{\parallel}$) and perpendicular ($I_{\perp}$) to the flow direction. Using 266-nm excitation, Raman bands of residue W26 in pVIII and of the bases in ssDNA are selectively enhanced, as indicated by the labels in Figure 7. The basis for these assignments has been established.[9−11,27,29] The computed difference spectrum, $I_{\parallel} - I_{\perp}$ shown in trace c, exhibits only positive peaks. Except for the diffuse feature at 1648 cm^{-1}, the positive peaks are assigned unambiguously to W26.[9,11] This is confirmed by the difference spectrum of *fd*(dW) in trace d of Figure 7. The weak positive difference intensity near 1648 cm^{-1} is probably due to incomplete compensation of the intense band near 1650 cm^{-1} which arises from both amide I and thymine.[29] The disappearance of the 1484-cm^{-1} adenine-plus-guanine band from the $I_{\parallel} - I_{\perp}$ spectrum of Figure 7 suggests that these bases either have no regular orientation in the hollow of the protein sheath or are configured such that their transition moments are directed close to the magic angle ($\psi \approx 52°$). While the absence of regularity in DNA base orientations would be consistent with the apparent absence of DNA contributions to the electron density map derived by X-ray diffraction,[7] and with solid state NMR data,[31] neither the present nor previous Raman results[9,11,29c] provide a definitive resolution of this question. Both *fd* structural models[32] and assembly mechanisms[33] have been proposed which imply some regularity in the ssDNA scaffold to which pVIII subunits

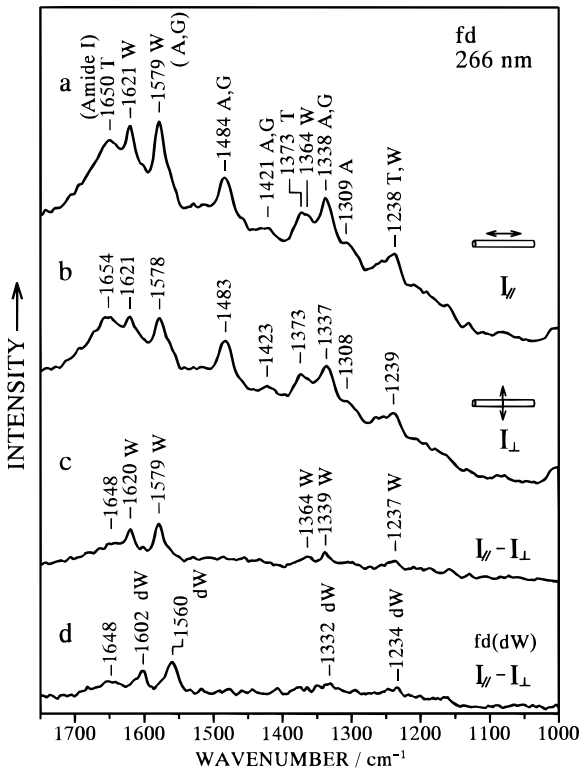

Figure 7. Resonance Raman spectra of the flow-oriented *fd* virus (1 mg/mL in 10 mM Tris) excited at 266 nm. The laser polarization is (a) parallel ($I_{\parallel}$), or (b) perpendicular ($I_{\perp}$) to the axis of alignment. Also shown is the Raman linear intensity difference, $I_{\parallel} - I_{\perp}$, for (c) normal *fd* virus and (d) *fd*(dW) virus, which incorporates deuteriotryptophan.

are attached. Further investigation of the structure of the packaged *fd* DNA molecule is required.

The intensity of the 1579-cm^{-1} band of tryptophan (ω2) in the 266-nm spectrum of *fd* arises from resonance with the L_a transition and provides information on the orientation of the transition moment with respect to the filament axis. However, with 266-nm excitation both adenine and guanine also contribute Raman intensity near 1580 cm^{-1}, equivalent to roughly half the intensity of the 1484-cm^{-1} band.[27] To compensate for these small purine contributions, the 266-nm Raman spectrum of a 6:5 mixture of deoxyadenosine 5′-monophosphate and deoxyguanosine 5′-monophosphate was subtracted from the $I_{\parallel}$ and $I_{\perp}$ spectra. Here, 6:5 represents the adenine:guanine ratio of *fd* DNA and the 1484-cm^{-1} band serves as an appropriate intensity standard. After the purine correction, we obtain $\gamma = 0.93$ for the reduced RLID of the 1579-cm^{-1} band using the expression on the left in eq 4. (A 13% lower value is obtained without the purine correction.)

Figure 8 shows Raman spectra excited at 240 nm on flow-oriented *fd* at $G = 3016$ s^{-1}. With 240-nm excitation, Raman bands of tyrosine (pVIII residues Y21 and Y24) as well as W26 are enhanced, whereas DNA base vibrations are not enhanced significantly. Only the DNA purine mode at 1488 cm^{-1} is observed in Figure 8, and as in the case of Figure 7, it is eliminated in the $I_{\parallel} - I_{\perp}$ difference spectrum. On the other hand, modes of tryptophan and tyrosine appear as positive bands in the difference spectrum. The difference peaks at 1463, 1362, 1341, 1202, and 1010 cm^{-1}, and to some extent the peak at 1620 cm^{-1}, are assigned to W26 on the basis of their known deuteration shifts.[9,11] (See also Figure 8d.) The remaining intensity differences at 1181 and 1620 cm^{-1} are ascribed to Y21

(28) (a) Berkowitz, S. A.; Day, L. A. *J. Mol. Biol.* **1976**, *102*, 531−547. (b) Newman, J.; Swinney, H. L.; Day, L. A. *J. Mol. Biol.* **1977**, *116*, 593−606.

(29) (a) Thomas, G. J., Jr.; Murphy, P. *Science* **1975**, *188*, 1205−1207. (b) Thomas, G. J., Jr.; Prescott, B.; Day, L. A. *J. Mol. Biol.* **1983**, *165*, 321−356. (c) Thomas, G. J., Jr.; Prescott, B.; Opella, S. J.; Day, L. A. *Biochemistry* **1988**, *27*, 4350−4357.

(30) Arnold, G. E.; Day, L. A.; Dunker, A. K. *Biochemistry* **1992**, *31*, 7948−7956.

(31) (a) Cross, T. A.; Tsang, P.; Opella, S. J. *Biochemistry* **1983**, *22*, 721−726. (b) Cross, T. A.; Opella, S. J. *J. Mol. Biol.* **1985**, *182*, 367−381. (c) Opella, S. J.; Stewart, P. L.; Valentine, K. G. *Q. Rev. Biophys.* **1987**, *19*, 7−49.

(32) (a) Marzec, C. J.; Day, L. A. *Biophys. J.* **1988**, *53*, 425−440. (b) Day, L. A.; Marzec, C. J.; Reisberg, S. A.; Casadevall, A. *Annu. Rev. Biophys. Biophys. Chem.* **1988**, *17*, 509−539.

(33) Webster, R. E. In *Phage Display of Peptides and Proteins*; Kay, B. K., Winter, J., McCafferty, J., Eds.; Academic Press: New York, in press.

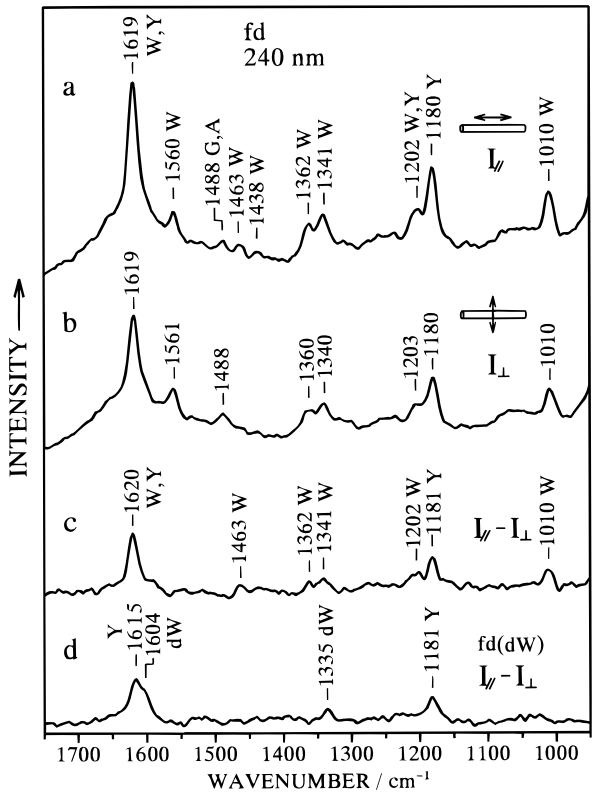

Figure 8. Resonance Raman spectra of the flow-oriented *fd* virus (1 mg/mL in 10 mM Tris) excited at 240 nm. The laser polarization is (a) parallel ($I_{\parallel}$), or (b) perpendicular ($I_{\perp}$) to the axis of alignment. Also shown is the Raman linear intensity difference, $I_{\parallel} - I_{\perp}$, for (c) normal *fd* virus and (d) *fd*(dW) virus, which incorporates deuteriotryptophan.

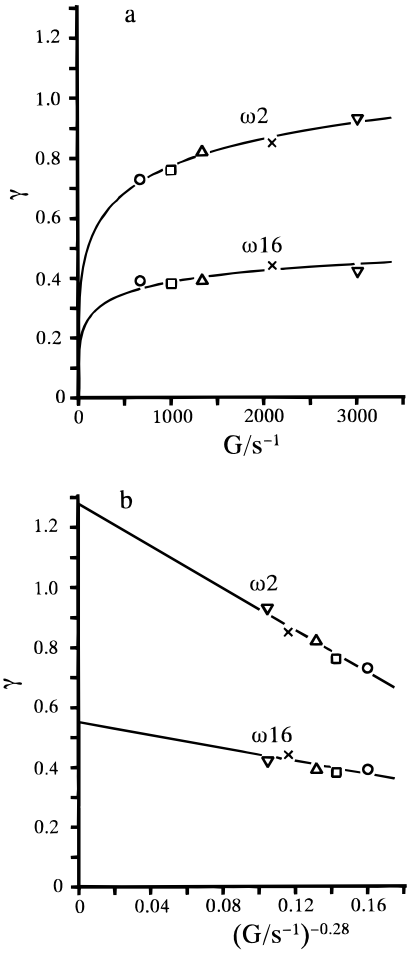

Figure 9. Plots of the reduced Raman linear intensity difference (γ) of the $\omega 2$ and $\omega 16$ bands of residue W26 against (a) the velocity gradient G and (b) $G^{-0.28}$. The straight lines in (b) represent least-squares fits of the data.

and Y24.[11] The $\omega 16$ band of tryptophan at 1010 cm^{-1} gains intensity through resonance with the B_b transition as described above. Since there is no significant overlap with other Raman bands in this frequency region (cf. Figure 8d), the reduced RLID for $\omega 16$ is calculated in straightforward manner from the observed $I_{\parallel}$ and $I_{\perp}$ spectra, yielding $\gamma = 0.42$.

RLID measurements were also made at lower velocity gradients, $G = 670$, 1005, 1340, and 2094 s^{-1}. The γ values obtained for $\omega 2$ (266 nm) and $\omega 16$ (240 nm) are plotted against G in Figure 9a. As noted above, the degree of alignment f, and therefore γ, should be proportional to $G^{-0.28}$ at high G. Figure 9b shows indeed that the plot of γ against $G^{-0.28}$ is linear for both $\omega 2$ and $\omega 16$. Extrapolation to infinite G gives $\gamma = 1.28 \pm 0.06$ for $\omega 2$ and 0.55 ± 0.10 for $\omega 16$. These values correspond to completely aligned *fd* filaments. By either eq 4 or the graphical $\gamma - \psi$ relationship of Figure 3, we obtain the following transition moment inclination angles: $\psi = 36.8 \pm 0.8°$ for the L_a band, and $\psi = 45.3 \pm 1.1°$ for the B_b band. Substitution of these ψ values and the observed γ values into eq 6 yields $f = 0.74 \pm 0.03$ as the degree of alignment when $G = 3016$ s^{-1}.

4. Orientation of the Indole Ring of Residue W26 in *fd*. The present RLID study has revealed the inclination angles of the L_a and B_b transition moments of the tryptophan residue W26 of the pVIII subunit with respect to the axis of the filamentous virus *fd*. Because the L_a and B_b absorptions arise from $\pi \rightarrow \pi^*$ transitions, the transition moments lie in the plane of the indole ring. In order to determine the indole ring orientation with respect to the virion axis, we require the directions of the L_a and B_b transition moments in the framework of the C3-substituted indole ring of tryptophan. Yamamoto and Tanaka[34] examined polarized absorption spectra of single crystals of 3-indolyl compounds and concluded that the L_a transition moment makes an angle of roughly −38° with the pseudo-2-fold axis (the line from indole atom C2 which bisects the C5−C6 bond of the indole ring). The negative value indicates an inclination toward the ring nitrogen atom. A more recent ultraviolet LD study by Albinsson and Nordén[35] on 3-methylindole in stretched polyethylene films determined that the L_a and B_b transitions are directed at $-44 \pm 1°$ and $11 \pm 10°$, respectively, from the pseudo-2-fold axis. Here we employ the transition moment directions reported by the latter authors.

Figure 10 illustrates the directions of the L_a and B_b transition moments within the plane of the indole ring of tryptophan. As determined by RLID, the L_a and B_b transition moments are inclined by $36.8 \pm 0.8°$ and $45.3 \pm 1.1°$, respectively, from the virion axis, i.e. the virion axis should make angles of 36.8 and 45.3° with the transition moments. The virion axis orientations which satisfy the former requirement define a cone around the L_a transition moment, and those satisfying the latter define a cone around the B_b transition moment. Intersections of the two cones represent virion axis orientations consistent with the data. As depicted in Figure 10, there are two such lines of intersection, which are directed symmetrically above and below the indole plane. The locations of the indole rings with respect to the lines of intersections represent two possible orientations, mutually related by reflection through a plane

(34) Yamamoto, Y.; Tanaka, J. *Bull. Chem. Soc. Jpn.* **1972**, *45*, 1362−1366.

(35) Albinsson, B.; Nordén, B. *J. Phys. Chem.* **1992**, *96*, 6204−6212.

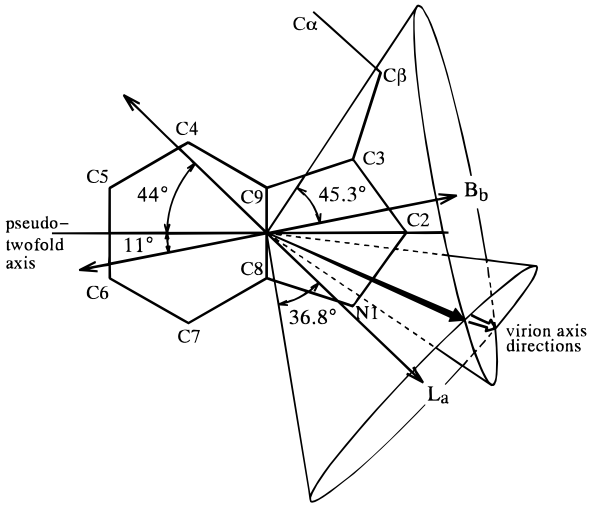

Figure 10. Directions of L_a and B_b transition moments in the plane of the indole ring of tryptophan (from ref 35) and cones showing allowed orientations of the *fd* virion axis with respect to the tryptophan transition moments. The lines of intersection of the cones, indicated by the filled and open arrows, indicate possible orientations of the virion axis with respect to the indole ring.

containing the virion axis. The two possible orientations cannot be distinguished experimentally by RLID. In either case, however, the plane of the indole ring is inclined at the relatively small angle of 31 ± 4° from the virion axis, and its pseudo-2-fold axis is inclined at 38 ± 6° with respect to the virion axis. Thus, the W26 indole ring of the *fd* coat protein subunit is roughly parallel to the virion axis.

Discussion

1. Orientation of Tryptophan Residue W26. Uniaxial alignment methods have been applied to filamentous viruses by several investigators. Bendet and Mayfield[36] examined the UVLD spectrum of flow-oriented *fd* and concluded that the aromatic rings of residues W26, Y21, and Y24 are roughly parallel to the virion axis while the planes of the DNA bases are approximately perpendicular to the axis. Fritzsche *et al.*[37] interpreted infrared LD spectra of oriented *fd* gels as indicative of coat protein α-helices nearly parallel to the virion axis. Torbet and Maret[38] measured optical birefringence of magnetically oriented *fd* gels and concluded that the α-helix and aromatics were close to parallel to the virion axis. Although these studies have provided qualitative information on *fd* architecture, quantitative conclusions could not be reached because of insufficient information on the degree of uniaxial alignment and/or incomplete information on the optical or magnetic properties of the chromophores.

More recently, Clack and Gray[39] measured UVLD spectra of *fd* at different flow rates and obtained an intrinsic LD spectrum corresponding to perfect alignment by extrapolating their data to infinite flow rate. The intrinsic LD spectrum in the region 250−310 nm was subsequently decomposed into contributions from DNA and protein, and inclination angles for "effective transition moments" of the DNA bases and pVIII aromatics (W26, Y21, Y24, F11, F42, F45) were calculated from the decomposed spectra. The putative inclination angles of the effective transition moments were regarded as upper limits for the virus. In this analysis, the LD signal of each chromophore was approximated as a constant multiple of the absorption intensity throughout the wavelength region examined. However, this approximation is subject to large uncertainties whenever the absorption band in question arises from multiple transitions with different polarization characteristics, as is the case for both the ssDNA bases and tryptophan residue of pVIII.

The pitfalls inherent in quantitative analysis of overlapping UV absorption bands of DNA and protein in filamentous viruses have been noted previously.[30,40] Because problems associated with band overlap are less serious for vibrational spectroscopy (particularly Raman and UVRR), and because the direction of a specific chromophore transition moment can be examined by selectively tuning the UVRR excitation wavelength, the RLID method offers unique advantages over UVLD. We have exploited these advantages to determine the orientation of the W26 indole ring of pVIII with respect to the virion axis. The present work represents the first quantitative determination of the W26 indole orientation in the *fd* virus at physiological solution concentration. In a complementary study, utilizing the polarization of Raman scattering in uniaxially oriented *fibers* of *fd*, Tsuboi *et al.*[12] have reported the determination of W26 indole orientation. The polarized Raman results on fibers and the RLID results on dilute solutions are in excellent agreement with one another. The consistency between solution and fiber determinations provides evidence that the molecular architecture of the *fd* assembly is invariant to any differences in inter-virion and virion−solvent interactions in the two morphological states examined.

2. Orientation of the α-Helical Subunit. The W26 orientation determined here (Figure 10) can be combined with the diagnostic Raman band, $\omega 3$, to estimate the local tilt angle, θ, of the pVIII α-helix in the vicinity of residue W26 with respect to the virion axis. The basis for this estimate is the following: The orientation of W26 with respect to the peptide main chain is governed by two dihedral angles, viz. χ^1 (N−Cα−Cβ−C3) and $\chi^{2,1}$ (Cα−Cβ−C3−C2). The latter is correlated with the precise frequency of the $\omega 3$ Raman band.[41] For the case of *fd*, the $\omega 3$ band is observed at 1560 cm^{-1} (Figure 8a), which indicates $|\chi^{2,1}| \approx 120°$.[9,11] Furthermore, due to steric requirements of α-helical structures, χ^1 is strictly dependent upon the $\chi^{2,1}$ dihedral angle,[42] i.e. $\chi^1 \approx -70°$ when $\chi^{2,1} \approx 120°$, and $\chi^1 \approx 180°$ when $\chi^{2,1} \approx -120°$.[42b] Model building supports this relationship between χ^1 and $\chi^{2,1}$ by revealing steric clashes whenever the pair (χ^1, $\chi^{2,1}$) deviates significantly from (−70°, 120°) and (180°, −120°).

We have calculated the helix tilt angle, θ, by using the permitted χ^1 and $\chi^{2,1}$ torsion angles (with allowances of ±10° uncertainty in both χ^1 and $\chi^{2,1}$), standard protein bond lengths and angles,[43] average Ramachandran angles (φ, ψ) for the α-helix main chain,[42b] and the two possible orientations of the indole ring with respect to the virion axis (Figure 10). The calculation has yielded $29° \le \theta \le 60°$ for (χ^1, $\chi^{2,1}$) = (−70 ± 10°, 120 ± 10°) and $41° \le \theta \le 88°$ for (χ^1, $\chi^{2,1}$) = (180 ± 10°, −120 ± 10°). The latter range may be rejected as incompatible with the body of available structural information, while the former is consistent with estimates based upon polarized Raman spectroscopy,[8] X-ray fiber diffraction,[7] solid

(36) Bendet, I. J.; Mayfield, J. E. *Biophys. J.* **1967**, *7*, 111−119.
(37) Fritzsche, H.; Cross, T. A.; Opella, S. J.; Kallenbach, N. R. *Biophys. Chem.* **1981**, *14*, 283−291.
(38) Torbet, J.; Maret, G. *Biopolymers* **1981**, *20*, 2657−2669.
(39) Clack, B. A.; Gray, D. M. *Biopolymers* **1992**, *32*, 795−810.
(40) Kostrikis, L. G.; Liu, D. J.; Day, L. A. *Biochemistry* **1994**, *33*, 1694−1703.
(41) (a) Miura, T.; Takeuchi, H.; Harada, I. *J. Raman Spectrosc.* **1989**, *20*, 667−671. (b) Maruyama, T.; Takeuchi, H. *J. Raman Spectrosc.* **1995**, *26*, 319−324.
(42) (a) Summers, N. L.; Carlson, W. D.; Karplus, M. *J. Mol. Biol.* **1987**, *196*, 175−198. (b) McGregor, M. J.; Islam, S. A.; Sternberg, M. J. E. *J. Mol. Biol.* **1987**, *196*, 295−310.
(43) Momany, F. A.; McGuire, R. F.; Burgess, A. W.; Scheraga, H. A. *J. Phys. Chem.* **1975**, *79*, 2361−2381.

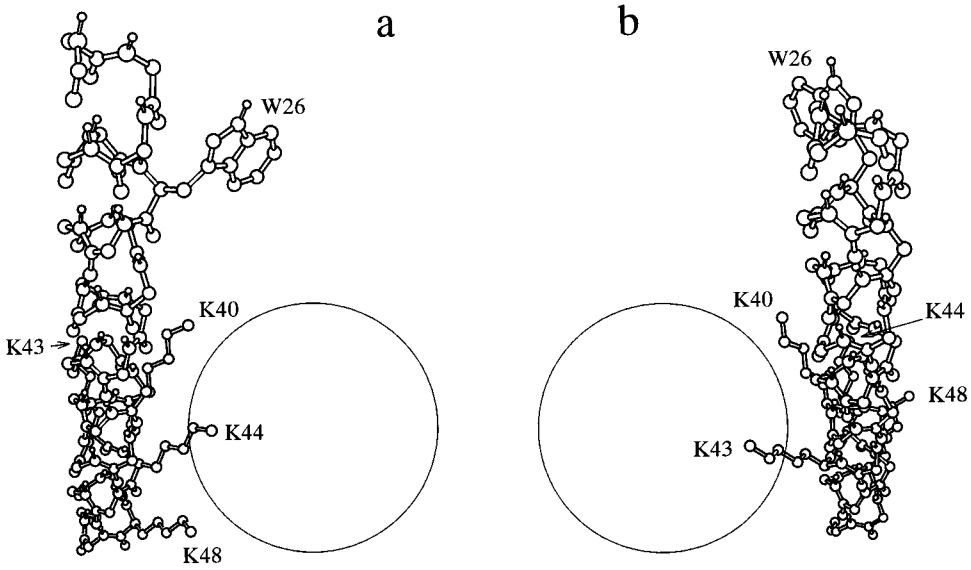

Figure 11. Two possible orientations of the *fd* coat protein subunit with respect to the virion axis, as viewed along the virion axis. The subunit is tilted with respect to the virion axis by 35° in (a) and 29° in (b). (See discussion in text.) For clarity only residues 21−50 are shown. Side chains are included for W26, K40, K43, K44, and K48. The circle represents a 20-Å core of the virion within which the packaged ssDNA genome resides.

state NMR,[31] magnetic birefringence,[38] and UVLD[39] results, all of which suggest that the α-helical subunits are aligned relatively close to parallel with the virion axis. Therefore, we adopt $\chi^1 = -70 \pm 10°$ and $\chi^{2,1} = 120 \pm 10°$ as the preferred W26 side chain torsions.

For the orientation of the indole ring corresponding to the virion axis direction represented by the filled arrow in Figure 10, we obtain $\theta = 35 \pm 10°$ when $(\chi^1, \chi^{2,1}) = (-80°, 110°)$ as the minimal tilt of the α-helix near residue W26. A second possibility is $\theta = 29 \pm 11°$ when $(\chi^1, \chi^{2,1}) = (-80°, 130°)$, which corresponds to the alternative virion axis direction (open arrow of Figure 10). The error limits of θ reflect the uncertainty of the indole ring orientation determined by RLID. Making the approximation that a similar tilt angle is propagated throughout the helix, we have constructed the two molecular models for the pVIII subunit shown in Figure 11, as viewed along the virion axis. For clarity, the N-terminal region (residues 1−20) and side chains other than W26, K40, K43, K44, and K48 are omitted. The lysines are believed accessible to DNA phosphates.[44] The lysine side chain conformation is assumed to be that most frequently found in α-helices.[42b] The circle (20-Å diameter) drawn in Figure 11 represents a plausible locus for the packaged ssDNA genome. In the pVIII model with $\theta = 35°$ (Figure 11a), the positively charged termini of K40, K44, and K48 are directed toward the presumed DNA core and the α-helix is tilted in a left-handed direction when viewed along a radius toward the virion axis. Conversely, for $\theta = 29°$ (Figure 11b), the α-helix has a right-handed tilt with respect to the virion axis and the main chain is rotated vis-à-vis Figure 11a by about 50° around the helix axis. This results in K40 and K43 being directed toward the DNA core. Interactions with DNA may also vary according to the conformations of the lysine side chains, curvature of the α-helical axis, and fraying of the helix in the vicinity of the C terminus.

The present model with $\theta = 29°$ (Figure 11b) is similar to a model proposed by Marvin and co-workers[7] on the basis of fiber X-ray diffraction analysis. In fact, slight curvature of the α-helix in the basic C-terminal domain and in the adjoining hydrophobic region is sufficient to very closely approximate the X-ray model, for which the helix inclination angle in the vicinity of residue W26 is 23° (Protein Data Bank, Identification Code 1IFJ[45]). Better agreement is obtained if the indole ring of W26 in the X-ray model[7] is rotated by approximately 180° around the Cβ−C3 axis to achieve consistency with the value of $\chi^{2,1}$ determined by Raman spectroscopy.[9,11] It is interesting to note that the RLID and X-ray methods indicate similar structure and orientation of the coat protein α-helix.

3. Orientation of Tyrosine Residues Y21 and Y24. The tyrosines (Y21 and Y24) of the *fd* subunit are revealed in the 240-nm UVRR spectrum of Figure 8 by their characteristic band near 1180 cm^{-1} (normal mode ν_{9a}). This band is well-resolved in the spectrum and is thus amenable to RLID analysis. The measured depolarization ratio ($\rho = 0.35 \pm 0.04$) is close to the value reported previously ($\rho = 0.39$) with 235-nm excitation.[26a] The ν_{9a} mode is considered to arise from nondegenerate **A**-term resonance with the L_a transition ($\lambda_{max} = 222$ nm) of the phenolic ring. Since the L_a transition moment is directed along the 2-fold axis of the ring, the polarized Raman intensity of the 1180-cm^{-1} band reflects the orientation of the 2-fold axis. We have analyzed the $I_{\|}$ and $I_{\perp}$ Raman intensities of the tyrosine ν_{9a} band in the manner described above for the tryptophan ω2 and ω16 bands. We obtain $\gamma = 0.91 \pm 0.08$ for perfectly aligned virus and $\psi = 41.2 \pm 0.9°$ for the angle between the 2-fold axis (L_a transition moment) and the virion axis. These results correspond to averages for residues Y21 and Y24, under the assumption that both contribute equally to the 1180-cm^{-1} band.

As in the case of W26, the tyrosine side chains of pVIII are expected to be restricted in their orientations by steric considerations for α-helices.[42] The preferred side chain torsions are $\chi^1 = 180 \pm 11°$ and $-73 \pm 14°$.[42b] Assuming a perfect α-helix, the value $\chi^1 = 180°$ would place the phenolic 2-fold axis (L_a) of Y21 at the angle $\psi = 71°$, and that of Y24 at an angle of 88° with respect to the virion axis. On the other hand, for $\chi^1 = -73°$, Y21 would have $\psi = 27°$, and Y24 would have $\psi = 46°$. Accordingly, the experimentally obtained average inclination angle ($\psi = 41.2°$) is best explained by a model in which both Y21 and Y24 adopt the side chain torsion $\chi^1 = -73°$. Finally, for $\chi^1 = -73°$, the torsion χ^2 may assume a wide range,

(44) (a) Hunter, G. J.; Rowitch, D. H.; Perham, R. N. *Nature (London)* **1987** *327*, 252−254. (b) Rowitch, D. H.; Hunter, G. J.; Perham, R. N. *J. Mol. Biol.* **1988** *204*, 663−674.

(45) Bernstein, F. C.; Koetzle, T. F.; Williams, G. J. B.; Meyer, E. F., Jr.; Bice, M. D.; Rodgers, J. R.; Kennard, O. *J. Mol. Biol.* **1977**, *112*, 535−542.

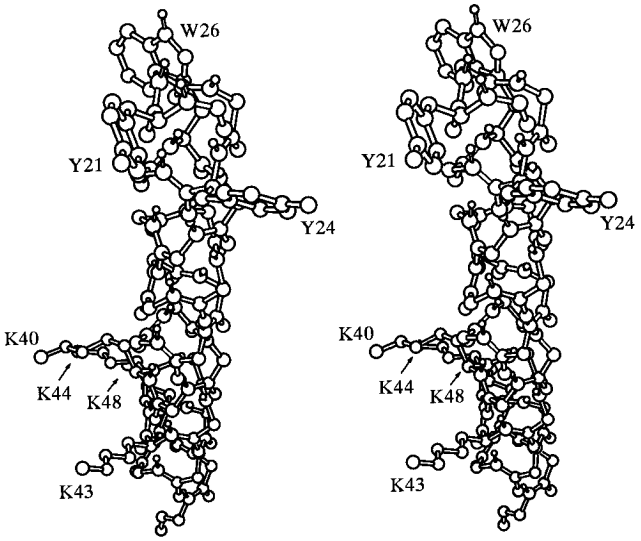

Figure 12. Stereo diagram of the proposed molecular model for the *fd* coat protein subunit viewed along the virion axis. The subunit orientation is that shown in Figure 11b. Side chains are included for W26, Y21, Y24, K40, K43, K44, and K48. Amino groups of the lysine side chains are available to interact with the DNA core.

viz. $102 \pm 46°$.[42b] Here, we assume $\chi^2 = 140°$ which avoids close contact of the phenolic ring with the main chain carbonyl oxygen. This preliminary determination of ring orientation for Y21 and Y24 will be confirmed in future RLID studies on single-site mutants of the virus in which each coat protein tyrosine has been mutated.[10]

4. Molecular Model for the *fd* Coat Protein Subunit. On the basis of the present results, we propose the molecular model shown in Figure 12 for the C-terminal sequence (residues 21−50) of the *fd* coat protein subunit. Orientations of the α-helix and W26 side chain are the same as illustrated in Figure 11b. The aromatic rings of both W26 and Y21 are close to parallel to the local α-helix axis, while the phenolic ring of Y24 is closer to perpendicular to the helix axis. The α-helix of Figure 12 has been twisted and curved slightly from the conformation depicted in Figure 11 by introducing incremental changes (−0.2°, +0.2°) in successive Ramachandran (ϕ, ψ) angles proceeding from residue 26 to the C terminus. Each lysine side chain conformation was selected from the permitted range[42b] so as to direct its terminal amino group toward the DNA core.

The present model for the main chain α-helix is consistent with the pVIII orientation determined by Overman *et al.*[8] on the basis of polarized Raman microspectroscopy of oriented *fd* fibers. The present α-helix model is also close to that determined by Marvin and co-workers[7] and is believed consistent with the X-ray fiber diffraction data. The side chain conformation for residue W26 determined here by the RLID method is likewise consistent with conclusions reached from polarized Raman microspectroscopy of oriented *fd* fibers.[12] The average orientations determined for Y21 and Y24 complement the conclusions reached from conventional solution Raman spectroscopy of wild type and mutant strains (Y21M and Y24M) of *Ff* virions.[10,11]

Because specific side chain orientations, such as those of tryptophan and tyrosine, are not revealed directly by X-ray analysis, improvement in X-ray based structural models[7] may result from the present findings. The present results may also help to elucidate interactions of coat protein subunits with one another and with the packaged ssDNA genome in native *Ff* assemblies.

Conclusions

We have developed and described a Raman linear intensity difference (RLID) method for determining orientations of chromophores in filamentous macromolecular assemblies. The present development involves use of a Couette flow cell to achieve *uniaxial orientation* of the filamentous particles and is based upon exploitation of the ultraviolet resonance Raman (UVRR) mechanism as a means of probing *specific transition moments* of *individual chromophores* in the biological assembly. Distinct advantages of the UVRR-RLID approach over conventional ultraviolet absorption linear dichroism (UVLD) result from the higher spectral resolution and sensitivity achievable with the former method.

The utility of the UVRR-RLID method has been demonstrated for the filamentous bacterial virus *fd*. Using 266- and 240-nm excitation of Raman spectra on flow-oriented *fd*, we have determined orientations of the L_a and B_b transition moments of the W26 residue of the viral coat protein subunit. By combining the transition moment orientations with known transition moment directions of the indole moiety, we have deduced the orientation of the W26 indole ring in the native *fd* virion in dilute aqueous solution. The results obtained on W26 are interpreted to suggest refinement of a recent molecular model of the virus proposed on the basis of fiber X-ray diffraction analysis. A similar procedure has been applied to determine the average orientations of Y21 and Y24 phenolic rings of the coat protein subunit.

In combination with a Raman band diagnostic of tryptophan side chain torsion, the UVRR-RLID results have also been interpreted to ascertain the orientation of the coat protein α-helix. A detailed molecular model has been developed from the RLID results.

The RLID methodology in combination with UVRR spectroscopy is a powerful tool for investigating chromophore structure in large biological assemblies, particularly when the assembly comprises multiple copies of a single protein and the sequence contains a single or a few identical chromophores resonant with a particular wavelength of laser excitation. Applications to other filamentous virus structures are in progress.

Acknowledgment. This research was supported under the Japan−U.S. Cooperative Science program by the Japan Society for the Promotion of Science and U.S. National Science Foundation (INT-9116242), and by research grants from the Ministry of Education, Science and Culture of Japan (No. 04640467 to H.T.) and U.S. National Institutes of Health (GM50776 to G.J.T.). The authors thank Professor Masamichi Tsuboi for valuable comments on the manuscript and for providing access to results prior to publication.

JA953923G